ACS OMEGA

Article

http://pubs.acs.org/journal/acsodf

Core–Shell Nanoparticles as an Efficient, Sustained, and Triggered Drug-Delivery System

Sonal Deshpande,[†] Sapna Sharma,[†] Veena Koul,[†,‡] and Neetu Singh*[,†,‡]

[†]Centre for Biomedical Engineering, Indian Institute of Technology-Delhi, Hauz Khas, New Delhi 110016, India

[‡]Biomedical Engineering Unit, All India Institute of Medical Sciences, Ansari Nagar, New Delhi 110029, India

Supporting Information

ABSTRACT: One of the challenges in designing a successful drug-delivery vehicle is the control over drug release. Toward this, a number of multifunctional nanoparticles with multiple triggers and complex chemistries have been developed. To achieve an efficient and maximum therapeutic effect, a trigger dependent drug-delivery system with sustained release is desirable. In this paper, we report the use of a combination of thermoresponsive gold core and polymeric shell nanoparticles that can provide a sustained, triggered release of doxorubicin, making the system more efficient compared to individual nanoparticles. The selection of the system was dependent on the best trigger applicable in biological systems and a component responsive to that trigger. Because of the best tissue penetration depth observed for radiofrequency (rf), we chose rf as a trigger. Whereas the gold nanoparticles (AuNPs) provided hyperthermia trigger on exposure to rf fields, the thermoresponsiveness was endowed by poly(*N*-isopropylacrylamide) (pNIPAm)-based polymer shells. AuNPs with three different compositions of shells, only pNIPAm and p(NIPAm-*co*-NIPMAm) with the ratio of NIPAm/*N*-(isopropylmethacrylamide) (NIPMAm) 1:1 (pNIPMAm$_{50}$) and 1:3 (pNIPMAm$_{75}$), were synthesized. We observed that the polymer coating on the AuNPs did not affect the heating efficiency of AuNPs by rf and exhibited a temperature-dependent release of the chemotherapeutic drug, doxorubicin. The nanoparticles were biocompatible, stable in biologically relevant media, and were able to show a burst as well as a sustained release, which was rf-dependent. Interestingly, we observed that when HeLa cells were treated with doxorubicin-loaded gold core–polymeric shell NPs and exposed to rf for varying times, the mixture of the two polymeric shell nanoparticles induced more cell death as compared to the cells treated with single nanoparticles, suggesting that such multi-nanoparticle systems can be more efficacious delivery systems instead of a single multicomponent system.

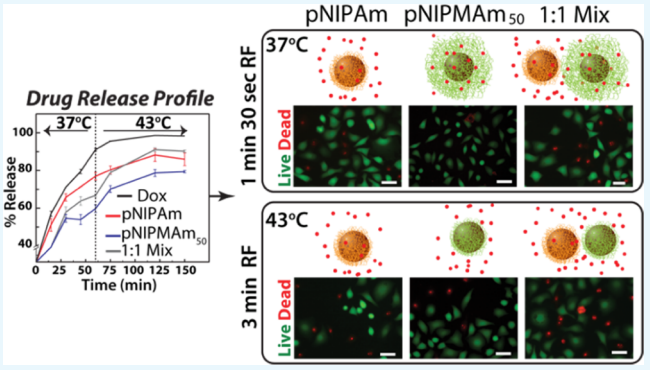

INTRODUCTION

Conventional drug therapy, though effective, mostly requires periodic administration of drugs at concentrations higher than that required at the target site, which can result in systemic toxicity. Moreover, its effectiveness is also highly dependent on patient compliance. To decrease the frequency of administration, dependence on patient compliance, and enhancing the effective concentration of the drug at the target site, nanocarriers are being exploited for drug delivery.[1,2] The basic properties considered while designing the nanocarriers are biocompatibility, drug-loading capacity, chemical handles for bioconjugation of targeting moieties, and control over the release kinetics of loaded drugs.

Most of the nanocarriers developed for drug delivery show a sustained release, where the release is governed by Fickian diffusion,[3] thereby providing least control over the release. Further efforts have led to the next generation "smart" nanocarriers, in which the release can be triggered in response to an endogenous or exogenous stimulus. The endogenous stimuli, such as pH,[4−6] redox,[7−9] hypoxia,[10] and enzymes,[11,12] are based on the microenvironment specific to the target sites. Because these triggers are continuously "ON", once activated, the system shows a continuous release. Alternatively, the exogenous triggers, such as temperature,[13] light,[14,15] magnetic field,[16] and electric current,[17] can provide advanced release profiles, also known as "on demand" release that follows "ON−OFF" signals. In fact, till date, a number of such nanocarriers, especially for delivery of nucleic acids, have been reported.[18] These systems utilize the difference in melting temperatures of different nucleic acid sequences for delivery, thereby making their application highly specific to nucleic acids.[19] Similarly, other systems such as nanogels are also being developed as switchable drug-delivery systems.[20,21] In the case of nanogels, where the release is dependent on deswelling and swelling properties, on exposure to the stimuli, most of the drug gets released from the system, thereby resulting in availability of a

Received: July 18, 2017
Accepted: September 25, 2017
Published: October 6, 2017

DOI: 10.1021/acsomega.7b01016
ACS Omega 2017, 2, 6455−6463

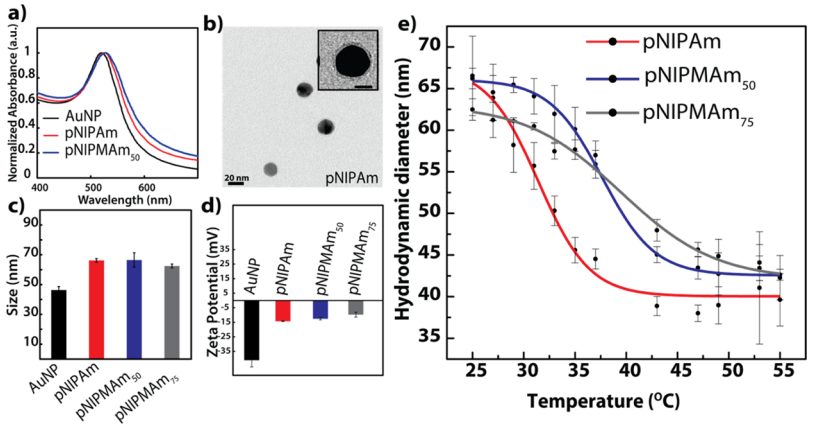

Figure 1. (a) Absorbance spectra of AuNPs and core−shells. (b) Transmission electron micrograph of AuNP−pNIPAm core−shell. Inset: Magnified image of the core−shell (scale = 10 nm). (c) Hydrodynamic diameter of the nanoparticles as measured by dynamic light scattering (DLS). (d) Zeta potential of the nanoparticles. (e) Effect of temperature on the hydrodynamic diameter of the core−shells analyzed by DLS. The error bars indicate the standard deviation between the triplicates. pNIPAm: Au core with the pNIPAm shell; $pNIPMAm_{50}$ and $pNIPMAm_{75}$: Au core with p(NIPAm-*co*-NIPMAm) shells with NIPAm/NIPMAm in the ratio of 1:1 and 1:3, respectively.

lower dose on the next trigger. Yet another approach pursued to achieve a triggered as well as sustained release is the synthesis of core−shell nanogels with varying degree of sensitivity to the stimuli.[22,23] However, introduction of multiple layers in such systems is challenging and perhaps involve complex chemistries. In addition, an increase in the number of layers adds to the complexity of drug release as well as tends to increase the overall size of the nanoparticles,[23] thus increasing the probability of clearance by the reticuloendothelial system. To overcome these, instead of incorporating complex or multiple components in a system to control the release profile, we propose a simple strategy of using a combination of nanoparticles, each having varying degrees of sensitivity to an exogenous trigger, thus obtaining a sustained, triggered release. We envision that such a strategy will allow us to achieve a sustained and triggered release as the trigger will have varied responses from multiple types of nanoparticles present in the solution. We hypothesize that single nanoparticles will be able to give an immediate or triggered burst release; if a combination of nanoparticles is used where at one condition, only one type of nanoparticle responds while the other remains dormant and responds at a different condition, then a dual responsive system can be developed from simple non-multifunctional nanoparticles. Such systems can also be helpful in the case of combinatorial therapies, for example, in the case of cancer treatment where the delivery of drugs for sensitizing cells to genotoxic drugs is necessary before the administration of genotoxic drugs to improve the overall efficiency of the treatment.[24]

As a proof of concept, here we report the use of a combination of thermoresponsive gold core−polymeric shell nanoparticles for demonstrating the sustained, triggered release of doxorubicin, a chemotherapeutic agent. Whereas the thermoresponsiveness was endowed by poly(*N*-isopropylacrylamide) (pNIPAm)-based polymer shells, the gold nanoparticles (AuNPs) provided a hyperthermia trigger on exposure to radiofrequency (rf) fields. pNIPAm is one of the well-studied thermoresponsive polymer, with the transition temperature close to the body temperature. In fact, the transition temperature of the polymer can be finely tuned by incorporation of different co-monomers such as acrylic acid, methacrylic acid, vinylacetic acid, *N*-(isopropylmethacrylamide) (NIPMAm), and so forth in the polymer backbone.[25] However, as the use of acids as a co-monomer also confers pH responsiveness to the nanogel, we selected NIPMAm for the shell synthesis. Though the biocompatibility of pNIPAm is one of the concerns limiting its clinical translation, it has been well-established that the toxicity observed in these systems is due to the monomer.[26] In fact, the polymer has been shown to be biocompatible at concentrations relevant to many biomedical applications. On the other hand, AuNPs are widely accepted for biomedical applications because of their bioinertness and biocompatibility.[2,27,28] They exhibit excellent optical resonance of their surface plasmons, resulting in strong absorbance at a characteristic wavelength and conversion of the resonance energy into heat. Although gold nanorods with surface plasmon resonance in the near-infrared (NIR) region have shown potential, their practical implementation is limited by the extent of tissue penetration (<2−3 cm).[29]Because the rf field has better penetration into the body[30] and is also known to efficiently heat the AuNPs in the size range of <50 nm,[31] research is now focused on the use of rf-mediated hyperthermia.

RESULTS AND DISCUSSION

We began our study by designing the dual component nanoparticle system for achieving a burst and a sustained release that can be modulated with a trigger. Usually, a multifunctional approach is utilized to develop a system capable of delivering cargoes in response to multiple triggers, thus leading to a sustained, triggered release. However, because multifunctionality in a single nanoparticle can result in various synthetic complexities[32] and can also impede the functionality, we developed a multi-nanoparticle system instead of a single multicomponent system. We explored a AuNP-based system that can heat up by application of an rf electric field. Because of their excellent ability to strongly absorb the light and efficiently convert the photon energy into heat, AuNPs are currently being exploited in photothermal therapy.[14,33] Recently, researchers have started investigating their ability to generate heat upon exposure to capacitively coupled rf electric fields. rf is of interest in the field of biomedicine, owing to its ability to penetrate deep into the tissues than the currently used NIR wavelengths.

DOI: 10.1021/acsomega.7b01016
ACS Omega 2017, 2, 6455−6463

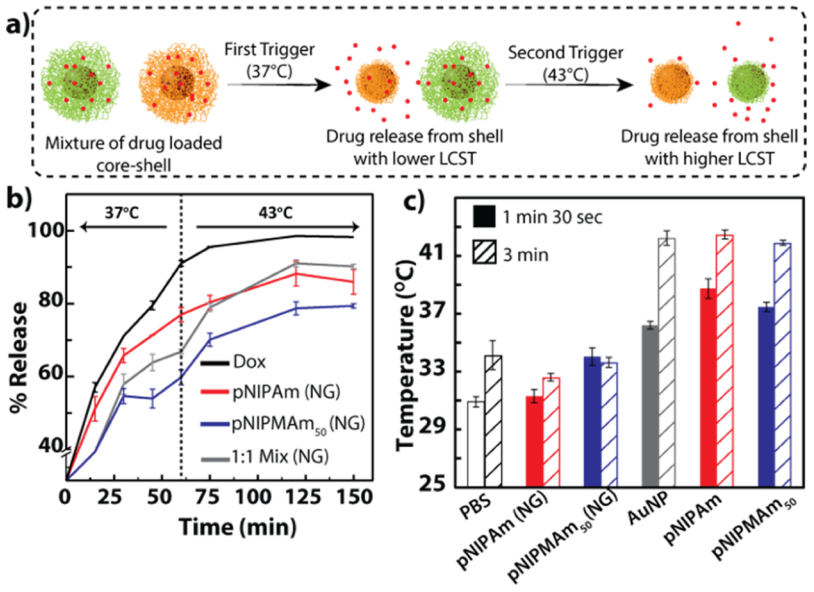

Figure 2. (a) Schematic representation of trigger-dependent sustained release of a drug from a mixture of nanoparticles having varying trigger sensitivities. (b) Release of doxorubicin from nanogels. The release was triggered after 60 min by increasing the temperature of the system from 37 to 43 °C (indicated by the dotted line). (c) rf-dependent heating of AuNPs and core−shell nanoparticles at 150 W. 1:1 mix: mixture of pNIPAm and $pNIPMAm_{50}$ nanoparticles in a 1:1 ratio; PBS: phosphate-buffered saline; pNIPAm: Au core with the pNIPAm shell; $pNIPMAm_{50}$: Au core with the p(NIPAm-*co*-NIPMAm) shell with NIPAm/NIPMAm in the ratio of 1:1; Dox: doxorubicin. NG indicates only nanogels with compositions corresponding to the shells in the core−shell nanoparticles.

A study by Moran et al. demonstrated the size-dependent heating efficiency and concluded that the AuNPs with <50 nm heated at twice the rate as compared to larger nanoparticles.[31] We therefore synthesized ∼20 nm AuNPs (via the well-reported Turkevich method), as evident from the single peak with absorption maxima at 520 nm (Figure 1a). The size was also confirmed by transmission electron microscopy (TEM) (Figure S2a). To render efficient drug-loading capabilities to the AuNPs, the commonly adapted strategies include direct adsorption of the active drug, surface deposition of charged polymers by the layer-by-layer (LBL) assembly, surface conjugation of thiolated amphiphilic polymers for generation of hydrophobic pockets for carrying drugs, and deposition of a porous shell for drug loading via absorption. The drug-loading efficiency by surface adsorption is limited by lack of inherent porosity of AuNPs, whereas the tendency of desorption and destabilization of polymeric layers because of protein interactions is a concern in LBL-assembled nanoparticles.[34] Although, surface conjugation of thiolated polymers can enhance the drug-loading efficiency, their sensitivity to intracellular glutathione (GSH) makes the system unsuitable for an externally controlled, triggered release.[9] We therefore opted for the porous shells for enhancing the drug-loading efficiency of our system. Additionally, as the trigger will result in the generation of heat (hyperthermia), a thermoresponsive polymer was desired. Importantly, the selection of appropriate temperatures for hyperthermia is crucial as the higher temperatures may cause irreversible cellular damage, leading to necrosis. This leads to a sudden release of necrotic cell contents, eventually giving rise to severe inflammatory responses. Typically, temperatures up to 45 °C[35] are preferred for hyperthermia as at this temperature, a series of subcellular events occur, which make the cells susceptible to damage without resulting in necrosis. Therefore, temperature-sensitive polymers, responsive at temperatures between 37 and 45 °C, were selected. As pNIPAm-based polymers exhibit thermoresponsive property near the physiological temperature, three core−shell nanoparticles with varying compositions of pNIPAm and pNIPMAm with *N*,*N*′-methylenebisacrylamide (BIS) as a cross-linker were synthesized via a well-known precipitation polymerization method. Whereas the cross-linker BIS concentration was constant (5 mol %), the compositions of the polymeric shells synthesized were only pNIPAm and poly(NIPAm-*co*-NIPMAm) with NIPAm/NIPMAm in the ratio of 1:1 and 1:3. These core−shell nanoparticles are named as pNIPAm, $pNIPMAm_{50}$, and $pNIPMAm_{75}$, respectively, in the manuscript.

After the synthesis of the polymer shell on AuNPs, a red shift of 5 nm was observed in the absorbance maxima, indicating successful surface modification of AuNPs (Figures 1a and S3). No significant change in the shape of the curve was observed, suggesting the absence of aggregation of the AuNPs, which otherwise may result in the attenuation of rf-dependent heating. The TEM images of the core−shells confirmed the absence of aggregation and the presence of a 2 ± 0.1 nm shell around the AuNP core (Figures 1b and S2). The nanoparticles were also characterized by DLS. The hydrodynamic diameter of AuNPs, pNIPAm, $pNIPMAm_{50}$, and $pNIPMAm_{75}$ was found to be 46 ± 2, 66 ± 1, 66.5 ± 5, and 62.5 ± 1 nm, respectively, at 25 °C (Figure 1c). The discrepancy observed in the sizes of the nanogels by TEM and DLS is as expected because DLS measures the hydrodynamic diameter, which is always greater than that observed by TEM. Also, as the samples are dried and imaged under vacuum for the TEM analysis, the shell tends to shrink, thereby further reducing the observed size in TEM. The surface charge of the AuNPs was negative with a reduction in the negative potential on shell formation (Figure 1d). We next investigated the lower critical solution temperature (LCST) of the synthesized nanoparticles, which is the temperature at which the polymer shell of the nanoparticle deswells. As observed in Figures 1e and S4, a significant change in the core−shell size was observed for pNIPAm at ∼32 °C, whereas

DOI: 10.1021/acsomega.7b01016
ACS Omega 2017, 2, 6455−6463

pNIPMAm$_{50}$ and pNIPMAm$_{75}$ showed size changes at around 39 and 40 °C, respectively. These changes in sizes can be considered significant, owing to the contribution of the AuNP core to the size of the core−shells. As the polymeric nanoparticles with more pNIPMAm composition (75 mol %) showed only 28% size reduction even at 47 °C, the temperature at which the cells could undergo necrosis, it was not considered for further studies. Thus, we envisioned that at a physiological temperature of 37 °C, pNIPAm would be deswollen and could be used for immediate release of the shell-loaded drug, whereas pNIPMAm$_{50}$ would be mostly dormant and release the drug only at an elevated temperature. Further, considering the deswelling observed for pNIPMAm$_{50}$, we selected a temperature between 32 and 45 °C, such that it is above the physiological temperature where pNIPAm would release the loaded drug and pNIPMAm$_{50}$ will retain, and at the same time it is below the necrosis temperature (45 °C). Additionally, to achieve a triggered release from pNIPMAm$_{50}$ above the physiological temperature, 43 °C was selected as the trigger temperature.

With two selected nanoparticles in hand, we proceeded to load doxorubicin, a potent chemotherapeutic agent, which works by intercalating with nucleic acids inside the cells, thereby inhibiting cell growth. Because of overlap of the absorbance spectra of doxorubicin and AuNPs and a low concentration of doxorubicin in the loaded samples, the loading efficiency was calculated by fluorescence intensities (ex 485/em 595 nm) after dissolving the AuNP core with aqua regia. As AuNPs have a broad absorbance spectrum, they can result in quenching of fluorescence signals.[36] Dissolving of the AuNP core was therefore necessary to eliminate its interference in measuring the doxorubicin fluorescence. The doxorubicin loading observed was comparable for core−shell nanoparticles, with 19% (192 μg/mg of core−shells) loading for pNIPAm and 14% (138 μg/mg of core−shells) for pNIPMAm$_{50}$. Additionally, it was also comparable to the doxorubicin loading observed in liposomes.[37,38] On the contrary, only ∼6% (65 μg/mg of AuNPs) loading was observed for AuNPs (Figure S5a). The loading was also confirmed by deconvolution of peaks in the absorbance spectra of doxorubicin-loaded core−shells (Figure S5b).

We first tested our hypothesis that a combination of nanoparticles can allow us to achieve a sustained release that can be increased by a temperature trigger (Figure 2a). We investigated the release profile of doxorubicin from nanogels of compositions corresponding to the polymeric shells using equilibrium dialysis. Doxorubicin-loaded pNIPAm, pNIPMAm$_{50}$, and 1:1 mixture of both the nanogels were dialyzed against PBS initially at 37 °C for 60 min, after which the temperature was increased to 43 °C. The initial burst release observed at 15 min can be attributed to doxorubicin adsorbed on the nanoparticle surface (Figure 2b). Further, as can be observed from the release profiles in Figure 2b, in the first 30 min, the release profile for pNIPAm (∼65%) was similar to that of the free doxorubicin control, indicating a burst release attributed to the deswelling of pNIPAm at 37 °C. Also, a comparatively less release (∼55%) was observed from pNIPMAm$_{50}$ initially, which then stabilized for upto 60 min, thus showing a sustained release behavior. Further, when the trigger was applied by increasing the temperature to 43 °C, pNIPAm showed no change in the release profile as against a significant increase in the drug release by pNIPMAm (∼30% increase) upto 150 min. Interestingly, the release profile for a 1:1 mixture of pNIPAm and pNIPMAm$_{50}$ showed an intermediate release profile at 37 °C, suggesting the immediate release effect due to deswelling of pNIPAm and retention of the drug by pNIPMAm$_{50}$. Further increase in temperature to 43 °C after 60 min resulted in an increase in the release, indicating the trigger-dependent additional release from pNIPMAm$_{50}$ of the mixture. Thus, the initial drug released from the mixture can provide an immediate effect, whereas a triggered release can provide an additional drug release from an otherwise sustained releasing system, thereby improving the overall efficiency of the system. These observations suggest that indeed a burst as well as a sustained drug-release profile that can be modulated with a trigger can be easily obtained by using a mixture of nanoparticles compared to the individual nanoparticles. To investigate the leakage of doxorubicin from the polymer shells, the release was also conducted at room temperature. As can be seen in Figure S6a, no significant difference was observed between pNIPAm and pNIPMAm at an early time point (20 min), whereas after 60 min, the overall release increased in either of the condition. However, a significant difference was observed between the release from pNIPAm and pNIPMAm nanoparticles at 37 °C. The diffusion of molecules from the nanoparticles is governed by the size and polymer cross-linking density of the nanoparticles. Reduction in the size enhances the rate of release, whereas an increase in the polymer cross-linking density slows the diffusion and hence retards the release. It is interesting to note that at 37 °C, as the pNIPAm core−shells significantly reduce in size, the diffusion can be easier, thus increasing the release. At 37 °C, the increase in the polymer density may retard the release in comparison with the release at room temperature, which is also observed in the data. For pNIPAm, retardation is observed at higher temperature because of slower diffusion due to increased polymer density, but eventually after 60 min, because of the smaller size, an overall increase in the release is observed. Although for pNIPMAm, a slight retardation is observed at higher temperature compared to that observed at room temperature, because the size does not change, there is no difference in the release over a longer period. We also investigated the effect of parameters such as cross-linking density,[39] pH,[40] and high GSH (10 mM),[41] which have a potential to influence the drug-release profiles. In this respect, core−shell nanoparticles with the shell composed of different cross-linking densities of bisacrylamide were synthesized. As can be observed in Figure S6b, at a low cross-linking density (1 mol % cross-linker), the release was faster than nanoparticles with a high cross-linking density (5 mol % cross-linker). Interestingly, a further increase in the cross-linking density did not show any significant difference in the release. Therefore, core−shells composed of 5 mol % bisacrylamide as the cross-linker were used for cell studies. Additionally, the drug release can also be affected by the acidic pH encountered by the nanoparticles in the tumor microenvironment or when the nanoparticles are internalized by the cells. Interestingly, though at an acidic pH, the overall release of doxorubicin was faster, pNIPMAm showed a less release compared to pNIPAm. The increase in the release rate can be attributed to the enhanced solubility of doxorubicin hydrochloride at an acidic pH (Figure S6c). On the other hand, GSH did not have a significant effect on the release of doxorubicin (Figure S6d).

After confirming the release profiles and advantage of using a combination of nanoparticles for achieving multiple release profiles, we evaluated the applicability of the nanoparticles as a drug-delivery system by studying its biocompatibility, hemo-

DOI: 10.1021/acsomega.7b01016
ACS Omega 2017, 2, 6455−6463

compatibility, stability in biologically relevant media, and ability to generate heat and release the drug on exposure to rf. We assessed the biocompatibility of gold core−polymeric shell nanoparticles by 3-(4,5-dimethylthiazol-2-yl)-2,5-diphenyltetrazolium bromide (MTT) assay using HeLa cells, a cervical cancer cell line. The nanoparticles did not show cytotoxicity at concentrations up to 0.3 nM (Figure S7a). The study on hemolytic activity of the nanoparticles also confirmed the biocompatibility of core−shells, as in all cases, the hemolysis was under 5% (FigureS7b). They were also stable in 10% fetal bovine serum (FBS) for up to 9 h, as observed by DLS (Figure S8). The release profile for doxorubicin loaded core−shells was then evaluated at different temperatures. As can be observed in Figure S9, after 60 min at 37 °C, pNIPAm showed 30 ± 2% release, whereas pNIPMAm$_{50}$ showed only 12 ± 3% release. When the system was maintained at 43 °C, an increase in the release was observed for pNIPMAm$_{50}$. This observation is in corroboration with the release study from the nanogel. Depending on these temperatures, we then optimized the rf (13.56 MHz, 150 W) exposure time for our system to attain the temperatures of 37 and 43 °C. Although a number of studies have shown the ability of AuNPs to generate heat on exposure to rf, the mechanisms underlying thermal dissipation are still not well-understood. Till date, three mechanisms, that is, Joules type heating, electrophoretic heating, and magnetic heating have been proposed.[42] The efficiency of thermal energy dissipation also depends on factors such as AuNP size, complexity of the medium, surface ligands, presence of salts, and rf instrument specifications.[31,43] Recently, a study by Li et al. demonstrated the influence of even the sample holder shape on the heating rate of AuNPs on rf exposure.[44] Thus, it is important to take into account these parameters while optimizing the exposure time and temperatures. Exposure of core−shells in a 96-well plate to rf (13.56 MHz) at 150 W with a standing wave ratio (SWR) close to 1 for 1 min 30 s resulted in the increase of temperature to 37 °C, whereas exposure for 3 min increased the temperature to 43 °C (Figure 2c). Interestingly, the surface modification of AuNPs by polymeric shells did not affect the heating rate of core−shell nanoparticles, and it was found to be similar to that of bare AuNPs (Figure S10). It is worth noting that PBS by itself also showed a slight increase in the temperature on exposure to rf, which was only 34 °C after 3 min of rf exposure. In addition, the temperature attained by corresponding composition nanogels was similar to that of PBS, suggesting that only AuNPs contribute to the heating on rf treatment (Figure 2c). The exposure times obtained from this study were then used for all cellular studies.

Finally, we evaluated the effect of a sustained and triggered release of shell-loaded doxorubicin from only pNIPAm, pNIPAM$_{50}$, and combination of the two nanoparticles on the HeLa cell line. The cells were treated with various nanoparticles while the doxorubicin concentrations were kept constant. After 4 h of incubation, the excess nanoparticles were removed from the culture media, and the cells with internalized nanoparticles were treated with rf for either 1 min 30 s or 3 min. Following the rf treatment, the cells were further cultured for 24 h, after which they were evaluated for cell viability via the MTT assay. It is well-known that AuNPs may interfere in the absorbance readout, but considering the very low concentration of AuNPs (upto 0.3 nM), we assume this effect to be negligible. As can be seen from Figure 3a, cells treated with nanoparticles without doxorubicin (controls) showed no cell death, whereas those treated with 0.7 μg/mL doxorubicin showed ∼50% cell death.

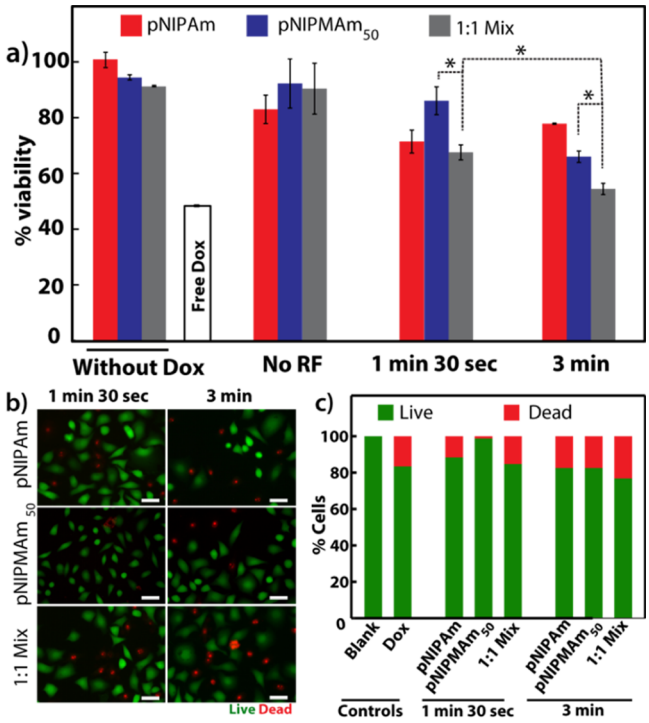

Figure 3. (a) Cell viability observed for doxorubicin-loaded core−shells on exposure to rf and analyzed by the MTT assay. (b) Live cell staining of HeLa cells treated with core−shell nanoparticles, exposed to rf and stained with calcein AM (green) and propidium iodide (PI, red) (scale = 50 μm). (c) Quantification of live−dead cells by fluorescence image analysis. Dox: doxorubicin; pNIPAm: core−shell with the pNIPAm shell; pNIPMAm$_{50}$: core−shell with the shell composed of a 1:1 ratio of NIPAm/NIPMAm; 1:1 mix: mixture of pNIPAm and pNIPMAm$_{50}$ core−shells in a 1:1 ratio; *: $P \leq 0.05$.

Additionally, cells treated either with pNIPMAm or the 1:1 combination of pNIPAm and pNIPMAm$_{50}$ nanoparticles did not show any cell death in the absence of the rf signal, whereas a slight reduction in the viability was observed for cells treated with pNIPAm because of the immediate release of doxorubicin into the medium at the cell culture temperature (37 °C). Similarly, comparable toxicity was observed for cells treated with pNIPAm and exposed to RF for 1 min 30 s and 3 min (Figure 3a), suggesting that all doxorubicin is probably released within 4 h of culture with nanoparticles. For the pNIPMAm$_{50}$-treated samples, a slight reduction in viability was observed at 1 min 30 s of rf treatment, which increased to ∼40% cell death with 3 min of rf treatment. The results observed can again be easily explained by the release profile curves observed in Figure 2b. As the cell culture temperature is well below the LCST of pNIPMAm$_{50}$, most of the doxorubicin is retained in the nanoparticle shell and released only after cellular internalization and upon rf application. As the short-time rf does not increase the temperature above the LCST, no significant decrease is observed compared to the 3 min rf where the temperature rises above the LCST, releasing doxorubicin intracellularly. The most striking results were obtained for samples treated with a combination of nanoparticles, where ∼67% cell viability was observed on 1 min 30 s of rf exposure, which reduced significantly to ∼50% cell death upon 3 min of rf exposure. The cell death observed was higher than either of the single nanoparticles. More importantly, the cell death in the combination was observed in response to the trigger as without

DOI: 10.1021/acsomega.7b01016
ACS Omega 2017, 2, 6455−6463

rf, no cytotoxicity was observed because of low amount of pNIPAm nanoparticles that can release the drug immediately. This allowed for most of the loaded drug to get internalized without causing unwanted nonspecific toxicity, which is desired for doxorubicin as it is known to induce a remarkable delayed cardiotoxicity.[45] With the combination, we get an advantage of an initial very low concentration release of doxorubicin at 37 °C, which acts as a first trigger, with the additional dose of doxorubicin being released specifically inside the cells after a second trigger on exposure to rf for 3 min. In the case of only pNIPAm and $pNIPMAm_{50}$, the effect can be termed as controlled release but not sustained, as all doxorubicin was released on exposure to the trigger, either the initial 37 °C or the second 43 °C. These studies clearly indicate that using a combination of nanoparticles, sensitive to a single trigger, can enhance the overall efficiency of the treatment and provide a controlled yet sustained release of doxorubicin.

We further confirmed the effect of doxorubicin on the cell viability by imaging live and dead cells after staining with calcein AM and PI (Figure 3b). Calcein AM is a nonfluorescent cell permeable dye, which is converted into a green fluorescent dye on hydrolysis by intracellular esterases, thereby staining only live cells, whereas PI, a cell impermeable dye, stains dead cells as their membrane gets compromised. After 1 min 30 s of rf exposure to the cells treated with doxorubicin-loaded nanoparticles, a few dead cells (red) were observed for pNIPAm as well as the 1:1 mixture, whereas most of the cells were live (green) for $pNIPMAm_{50}$ nanoparticles. On 3 min of rf exposure, maximum dead cells were observed for cells treated with a 1:1 mixture of nanoparticles. The fluorescence images were also used for quantification by counting the live and dead cells in at least three representative areas of each sample (Figure 3c). The results obtained were in agreement with the cell viability analysis by the MTT assay and confirm the enhanced efficiency of drug delivery in a mixture of nanoparticles as against individual nanoparticles.

CONCLUSIONS

Our study suggests a simple alternative to the development of nanoparticles via complex chemistries for endowing one of the most important properties for drug delivery, that is, sustained, triggered release of the loaded drug. Whereas the single nanoparticles did result in cell death, the effect was enhanced by using a mixture of nanoparticles. $pNIPMAm_{50}$ showed a pronounced effect in response to exposure to longer rf hyperthermia period (3 min), which was improved on using them as a mixture with the pNIPAm-based shell, suggesting the potential of this concept of using a multi-nanoparticle system as a more efficacious vehicle instead of single multicomponent vehicles.

EXPERIMENTAL SECTION

Materials. Gold(III) chloride trihydrate ($HAuCl_4$), sodium citrate tribasic dihydrate, amine-terminated pNIPAm (average M_n 2500), NIPAm, and NIPMAm were obtained from Sigma-Aldrich. Sodium dodecyl sulfate (SDS) was obtained from Merck. Ammonium persulfate (APS) and BIS were obtained from Loba Chemie. Doxorubicin hydrochloride (Adriamycin) was procured from Pfizer. HeLa cells were obtained from the National Centre for Cell Sciences, Pune, India. Dulbecco's modified Eagle medium (DMEM, high glucose), Dulbecco's phosphate-buffered saline, calcein AM, trypsin, FBS, and MTT were procured from Thermo Fisher Scientific.

AuNP (Core) Synthesis. AuNPs were synthesized using the well-known Turkevich method.[46] All glassware and Teflon-coated magnetic beads were first cleaned with aqua regia and rinsed thoroughly with deionized water. Under vigorous stirring, 190 mL of 0.1 mg/mL $HAuCl_4$ solution was brought to boil in a round-bottom flask attached with a condenser. $HAuCl_4$ was then reduced by addition of 10 mL of 1% sodium citrate trihydrate. The solution turned from dark purple to red wine color within 10 min and was stirred for another 20 min. It was then brought to room temperature with continuous stirring. Then, the formed AuNPs were characterized by ultraviolet−visible (UV−vis) absorbance spectroscopy, DLS, and TEM. The size obtained by the TEM analysis and the corresponding molar extinction coefficient[47] were used to calculate the AuNP concentration by using the Beer−Lambert law.

Nanogel (Shell) Synthesis. AuNPs coated with amine-terminated pNIPAm (pNIPAm-NH_2) were used as the seed for the shell synthesis. As excess of the polymer can result in the aggregation of AuNPs,[48] we first optimized the amount of pNIPAm-NH_2 that can be used for coating (Figure S1). AuNPs (1 nM) were incubated with increasing concentration of pNIPAm-NH_2 (2500 Da) for 6 h, and their absorbance spectra were recorded. As the aggregation occurred at concentrations above 3 μM (Figure S1), this concentration was used for coating the AuNPs. Also, as a free polymer can result in the formation of nanogels without the AuNP core, as a precaution, the nanoparticles were dialyzed against deionized water using a 12 kDa dialysis membrane for 4 h to remove any free unabsorbed pNIPAm-NH_2.

The nanogel shells were then synthesized by precipitation polymerization using pNIPAm-NH_2-coated AuNPs as the seed, according to a previously reported method.[49] Briefly, for a 40 mL reaction, an appropriate amount of monomers, NIPAm and NIPMAm, cross-linker, BIS, and 130 μL of SDS (0.1 M) were added to the seed. SDS, an anionic surfactant, is known to be involved in the early stabilization of nuclei generated during the synthesis, leading to a reduction in the size of the pNIPAm nanogels.[50] The mixture was heated to 70 °C under a N_2 environment with stirring for 1 h. Freshly prepared APS (260 μL of 0.1 M) was then injected to initiate the reaction. After ∼20 min, turbidity was observed, indicating polymer formation. The reaction was continued for 4 h and was cooled down to room temperature with continuous stirring. The core−shell nanoparticles were then washed three times with deionized water by centrifuging at 12 000 rpm for 15 min. Different shell compositions used were (i) 95 mol % NIPAm and 5 mol % BIS (pNIPAm), (ii) 45 mol % NIPAm, 50 mol % NIPMAm, and 5 mol % BIS ($pNIPMAm_{50}$), and (iii) 75 mol % NIPMAm, 20 mol % NIPAm, and 5 mol % BIS ($pNIPMAm_{75}$), with a total monomer concentration of 20 mM. Similarly core−shells with 10, 5, and 1 mol % BIS cross-linker densities were also synthesized. The core−shell nanoparticles were characterized by UV−vis spectroscopy for the aggregation of AuNPs and shell formation by TEM. Shell formation was also confirmed by monitoring the temperature-dependent size of the nanoparticles as analyzed by DLS.

Drug Loading and Loading Efficiency. The nanoparticles were centrifuged at 12 000 rpm for 15 min. The pellet was then resuspended in 200 μL of 1 mg/mL doxorubicin hydrochloride solution such that the concentration

DOI: 10.1021/acsomega.7b01016
ACS Omega 2017, 2, 6455−6463

of core−shell nanoparticles was 15 nM. They were then incubated overnight and washed twice with deionized water by centrifugation to remove the unabsorbed drug. Drug loading was confirmed by absorbance and fluorescence spectroscopy.

The loading efficiency was calculated by fluorescence spectroscopy. As the AuNP core interfered with the fluorescence of doxorubicin, they were first digested with aqua regia, and then the obtained fluorescence was used to calculate the amount of doxorubicin, using the equation obtained from a standard plot of doxorubicin in the presence of aqua regia. It should be noted that the fluorescence of doxorubicin is affected by aqua regia and decreases with time (data not shown). It is therefore necessary to record the fluorescence immediately after addition of aqua regia. The amount of nanoparticles used for loading was determined by drying a known concentration of core−shells. The following formula was used for calculating the loading efficiency

$$\%\ \text{loading} = \frac{\text{amount of doxorubicin loaded (mg)}}{\text{amount of nanoparticles (mg)}} \times 100$$

Temperature-Dependent Drug Release. The release profile of doxorubicin from nanoparticles was performed at room temperature, 37, and 43 °C by equilibrium dialysis. The release at different pH values and with core−shells composed of different cross-linking densities were carried out at 37 °C. The samples were dialyzed using a 12 kDa cellulose membrane against PBS. For release at acidic pH, PBS at pH 5 was used as a release medium. They were aliquoted at different time intervals and analyzed for doxorubicin fluorescence. The percentage release was calculated using the following formula:

$$\%\ \text{release} = 100 - \left(\frac{\text{fluorescence of sample at time } t}{\text{fluorescence of sample at time zero}} \times 100 \right)$$

rf-Assisted Hyperthermia. A custom-made 13.56 MHz rf generator was used for the experiments. It was operated at a power of 150 W while keeping the SWR close to 1. The SWR helps in adjusting the reflected power value of the total rf power. The samples were prepared in PBS, brought to room temperature (∼25 °C), and were exposed to rf for different times. At the end of the exposure, the temperature of the core−shell nanoparticles was immediately determined by a digital thermometer. The values obtained were plotted against time to obtain the heating rate.

Cell Viability by the MTT Assay. Cervical cancer cell lines, HeLa, were cultured in DMEM media supplemented with 10% FBS and incubated at 37 °C and 5% CO_2 in a CO_2 incubator. At ∼80% confluency, the cells were trypsinized, and 10^4 cells were seeded in each well of a 96-well plate and cultured overnight. The media was removed, and fresh media containing UV-sterilized, doxorubicin-loaded nanoparticles at varying concentrations were added over the cells. The cells were then incubated, and after 4 h, the nanoparticle-containing media were replaced with 40% FBS in deionized water. They were then exposed to the rf field at 150 W for 1 min 30 s and 3 min. FBS was then replaced with fresh DMEM + 10% FBS and further incubated for 24 h. The media was then removed, and fresh media containing MTT at a final concentration of 0.5 mg/mL was added over the cells. After 1 h of incubation, the media was removed, and the insoluble formazan crystals synthesized by the live cells were dissolved in 200 μL of dimethyl sulfoxide. Absorbance of the solution was then recorded at 550 nm using a BioTek SynergyH1 multiplate reader. Cells not treated with nanoparticles were considered as blank and used to calculate the percentage viability for nanoparticle-treated cells. Cells treated with nanoparticles without doxorubicin were used as controls.

Hemolysis Assay. Hemolysis assay was performed by adding core−shells at different concentrations to 50 μL of erythrocytes to a final volume of 250 μL in PBS. After incubation at 37 °C for 30 min, the cells were centrifuged at 10 000*g* for 5 min, and the absorbance of the supernatant was measured at 540 nm to quantify the cell lysis. Cells untreated with nanoparticles were used as the negative control, and the cells incubated with 10% Triton X-100 were used as the positive control.

Live Cell Staining. HeLa cells were seeded in a 96-well plate at a seeding density of 10^4 cells per well and cultured overnight at 37 °C under 5% CO_2. UV-sterilized, doxorubicin-loaded nanoparticles were diluted in fresh media, such that the final concentration of doxorubicin was 0.7 μg/mL, and added over the cells. The cells were then incubated for 4 h, and the media was replaced with 40% FBS in deionized water. One 96-well plate was exposed to rf (150 W) for 1 min 30 s and other was exposed for 3 min. FBS was then replaced with fresh DMEM + 10% FBS and further incubated for 24 h. The media was then removed and fresh media containing 2 μM calcein AM, a live cell stain, and 2 μM propidium iodide were added over the cells. After 20 min of incubation, the cells were washed and imaged under an Olympus IX73 inverted microscope using fluorescein isothiocyanate and PI filters. The cells without nanoparticle treatment were used as blank.

■ ASSOCIATED CONTENT

Supporting Information

The Supporting Information is available free of charge on the ACS Publications website at DOI: 10.1021/acsomega.7b01016.

Transmission electron micrographs of AuNPs and core−shells, doxorubicin-loading efficiency, biocompatibility by MTT and haemolysis assays, serum stability, drug-release profile, and heating rate of core−shells (PDF)

■ AUTHOR INFORMATION

Corresponding Author

*E-mail: sneetu@iitd.ac.in. Phone: +91-011-26591422. Fax: +91-11-26582037 (N.S.).

ORCID

Neetu Singh: 0000-0002-7880-4880

Author Contributions

The manuscript was written through contributions of all authors. All authors have given approval to the final version of the manuscript.

Notes

The authors declare no competing financial interest.

■ ACKNOWLEDGMENTS

We acknowledge financial support by the Indian Institute of Technology, Delhi, India, through the Industrial Research and Development Unit (MI01147) and the Planning Unit. The work was funded by the DST-Nanomission, India (SR/NM/NS-1022/2013). S.D. acknowledges the SRF fellowship support

DOI: 10.1021/acsomega.7b01016
ACS Omega 2017, 2, 6455−6463

from the UGC, India. We gratefully acknowledge Chetan Nehate for his assistance in using the RF instrument. We also acknowledge the Central Research Facility, IIT, Delhi and the Nanoscale Research Facility, IIT, Delhi for TEM and DLS, respectively.

■ ABBREVIATIONS

NIPAm, AuNP core with the pNIPAm shell; $pNIPMAm_{50}$, AuNP core with the p(NIPAm-*co*-NIPMAm) shells with NIPAm/NIPMAm in 1:1; Dox, doxorubicin; 1:1 mix, mixture of pNIPAm and $pNIPMAm_{50}$ nanoparticles in 1:1 ratio; $pNIPMAm_{75}$, AuNP core with the p(NIPAm-*co*-NIPMAm) shell with NIPAm/NIPMAm in 1:3 ratio

■ REFERENCES

(1) Bao, G.; Mitragotri, S.; Tong, S. Multifunctional nanoparticles for drug delivery and molecular imaging. *Annu. Rev. Biomed. Eng.* **2013**, *15*, 253−282.
(2) Kim, C.-k.; Ghosh, P.; Rotello, V. M. Multimodal drug delivery using gold nanoparticles. *Nanoscale* **2009**, *1*, 61−67.
(3) Mura, S.; Nicolas, J.; Couvreur, P. Stimuli-responsive nanocarriers for drug delivery. *Nat. Mater.* **2013**, *12*, 991−1003.
(4) Deng, Z.; Zhen, Z.; Hu, X.; Wu, S.; Xu, Z.; Chu, P. K. Hollow chitosan−silica nanospheres as pH-sensitive targeted delivery carriers in breast cancer therapy. *Biomaterials* **2011**, *32*, 4976−4986.
(5) Muhammad, F.; Guo, M.; Qi, W.; Sun, F.; Wang, A.; Guo, Y.; Zhu, G. pH-Triggered Controlled Drug Release from Mesoporous Silica Nanoparticles via Intracelluar Dissolution of ZnO Nanolids. *J. Am. Chem. Soc.* **2011**, *133*, 8778−8781.
(6) Min, K. H.; Kim, J.-H.; Bae, S. M.; Shin, H.; Kim, M. S.; Park, S.; Lee, H.; Park, R.-W.; Kim, I.-S.; Kim, K.; Kwon, I. C.; Jeong, S. Y.; Lee, D. S. Tumoral acidic pH-responsive MPEG-poly(β-amino ester) polymeric micelles for cancer targeting therapy. *J. Controlled Release* **2010**, *144*, 259−266.
(7) Li, Y.; Xiao, K.; Luo, J.; Xiao, W.; Lee, J. S.; Gonik, A. M.; Kato, J.; Dong, T. A.; Lam, K. S. Well-defined, reversible disulfide cross-linked micelles for on-demand paclitaxel delivery. *Biomaterials* **2011**, *32*, 6633−6645.
(8) Kim, H.; Kim, S.; Park, C.; Lee, H.; Park, H. J.; Kim, C. Glutathione-Induced Intracellular Release of Guests from Mesoporous Silica Nanocontainers with Cyclodextrin Gatekeepers. *Adv. Mater.* **2010**, *22*, 4280−4283.
(9) Wang, X.; Cai, X.; Hu, J.; Shao, N.; Wang, F.; Zhang, Q.; Xiao, J.; Cheng, Y. Glutathione-triggered "off−on" release of anticancer drugs from dendrimer-encapsulated gold nanoparticles. *J. Am. Chem. Soc.* **2013**, *135*, 9805−9810.
(10) Thambi, T.; Deepagan, V. G.; Yoon, H. Y.; Han, H. S.; Kim, S.-H.; Son, S.; Jo, D.-G.; Ahn, C.-H.; Suh, Y. D.; Kim, K.; Kwon, I. C.; Lee, D. S.; Park, J. H. Hypoxia-responsive polymeric nanoparticles for tumor-targeted drug delivery. *Biomaterials* **2014**, *35*, 1735−1743.
(11) Xu, J.-H.; Gao, F.-P.; Li, L.-L.; Ma, H. L.; Fan, Y.-S.; Liu, W.; Guo, S.-S.; Zhao, X.-Z.; Wang, H. Gelatin−mesoporous silica nanoparticles as matrix metalloproteinases-degradable drug delivery systems in vivo. *Microporous Mesoporous Mater.* **2013**, *182*, 165−172.
(12) Lee, G. Y.; Qian, W. P.; Wang, L.; Wang, Y. A.; Staley, C. A.; Satpathy, M.; Nie, S.; Mao, H.; Yang, L. Theranostic Nanoparticles with Controlled Release of Gemcitabine for Targeted Therapy and MRI of Pancreatic Cancer. *ACS Nano* **2013**, *7*, 2078−2089.
(13) Rastogi, R.; Gulati, N.; Kotnala, R. K.; Sharma, U.; Jayasundar, R.; Koul, V. Evaluation of folate conjugated pegylated thermosensitive magnetic nanocomposites for tumor imaging and therapy. *Colloids Surf., B* **2011**, *82*, 160−167.
(14) Cheng, Y.; Doane, T. L.; Chuang, C.-H.; Ziady, A.; Burda, C. Near Infrared Light-Triggered Drug Generation and Release from Gold Nanoparticle Carriers for Photodynamic Therapy. *Small* **2014**, *10*, 1799−1804.
(15) Bao, Z.; Liu, X.; Liu, Y.; Liu, H.; Zhao, K. Near-infrared light-responsive inorganic nanomaterials for photothermal therapy. *Asian J. Pharm. Sci.* **2016**, *11*, 349−364.
(16) Dionigi, C.; Piñeiro, Y.; Riminucci, A.; Bañobre, M.; Rivas, J.; Dediu, V. Regulating the thermal response of PNIPAM hydrogels by controlling the adsorption of magnetite nanoparticles. *Appl. Phys. A: Mater. Sci. Process.* **2014**, *114*, 585−590.
(17) Tamarov, K. P.; Osminkina, L. A.; Zinovyev, S. V.; Maximova, K. A.; Kargina, J. V.; Gongalsky, M. B.; Ryabchikov, Y.; Al-Kattan, A.; Sviridov, A. P.; Sentis, M.; Ivanov, A. V.; Nikiforov, V. N.; Kabashin, A. V.; Timoshenko, V. Y. Radio frequency radiation-induced hyperthermia using Si nanoparticle-based sensitizers for mild cancer therapy. *Sci. Rep.* **2014**, *4*, 7034.
(18) Rajendrakumar, S.; Uthaman, S.; Cho, C.; Park, I.-K. Trigger-Responsive Gene Transporters for Anticancer Therapy. *Nanomaterials* **2017**, *7*, 120.
(19) Derfus, A. M.; von Maltzahn, G.; Harris, T. J.; Duza, T.; Vecchio, K. S.; Ruoslahti, E.; Bhatia, S. N. Remotely Triggered Release from Magnetic Nanoparticles. *Adv. Mater.* **2007**, *19*, 3932−3936.
(20) Molina, M.; Giulbudagian, M.; Calderón, M. Positively Charged Thermoresponsive Nanogels for Anticancer Drug Delivery. *Macromol. Chem. Phys.* **2014**, *215*, 2414−2419.
(21) Shin, Y.; Chang, J. H.; Liu, J.; Williford, R.; Shin, Y.-K.; Exarhos, G. J. Hybrid nanogels for sustainable positive thermosensitive drug release. *J. Controlled Release* **2001**, *73*, 1−6.
(22) Kotsuchibashi, Y.; Narain, R. Dual-temperature and pH responsive (ethylene glycol)-based nanogels via structural design. *Polym. Chem.* **2014**, *5*, 3061−3070.
(23) Zhang, J.; Yang, F.; Shen, H.; Wu, D. Controlled Formation of Microgels/Nanogels from a Disulfide-Linked Core/Shell Hyperbranched Polymer. *ACS Macro Lett.* **2012**, *1*, 1295−1299.
(24) Lee, M. J.; Ye, A. S.; Gardino, A. K.; Heijink, A. M.; Sorger, P. K.; MacBeath, G.; Yaffe, M. B. Sequential Application of Anticancer Drugs Enhances Cell Death by Rewiring Apoptotic Signaling Networks. *Cell* **2012**, *149*, 780−794.
(25) Burmistrova, A.; Richter, M.; Eisele, M.; Üzüm, C.; von Klitzing, R. The Effect of Co-Monomer Content on the Swelling/Shrinking and Mechanical Behaviour of Individually Adsorbed PNIPAM Microgel Particles. *Polymers* **2011**, *3*, 1575−1590.
(26) Malonne, H.; Eeckman, F.; Fontaine, D.; Otto, A.; De Vos, L.; Moës, A.; Fontaine, J.; Amighi, K. Preparation of poly(N-isopropylacrylamide) copolymers and preliminary assessment of their acute and subacute toxicity in mice. *Eur. J. Pharm. Biopharm.* **2005**, *61*, 188−194.
(27) Ghosh, P.; Han, G.; De, M.; Kim, C.; Rotello, V. Gold nanoparticles in delivery applications. *Adv. Drug Delivery Rev.* **2008**, *60*, 1307−1315.
(28) Jeong, E. H.; Jung, G.; Hong, C. A.; Lee, H. Gold nanoparticle (AuNP)-based drug delivery and molecular imaging for biomedical applications. *Arch. Pharmacal Res.* **2014**, *37*, 53−59.
(29) Arnfield, M. R.; Mathew, R. P.; Tulip, J.; McPhee, M. S. Analysis of tissue optical coefficients using an approximate equation valid for comparable absorption and scattering. *Phys. Med. Biol.* **1992**, *37*, 1219.
(30) Gannon, C. J.; Cherukuri, P.; Yakobson, B. I.; Cognet, L.; Kanzius, J. S.; Kittrell, C.; Weisman, R. B.; Pasquali, M.; Schmidt, H. K.; Smalley, R. E.; Curley, S. A. Carbon nanotube-enhanced thermal destruction of cancer cells in a noninvasive radiofrequency field. *Cancer* **2007**, *110*, 2654−2665.
(31) Moran, C. H.; Wainerdi, S. M.; Cherukuri, T. K.; Kittrell, C.; Wiley, B. J.; Nicholas, N. W.; Curley, S. A.; Kanzius, J. S.; Cherukuri, P. Size-dependent joule heating of gold nanoparticles using capacitively coupled radiofrequency fields. *Nano Res.* **2009**, *2*, 400−405.
(32) Fan, L.; Zhang, Y.; Wang, F.; Yang, Q.; Tan, J.; Grifantini, R.; Wu, H.; Song, C.; Jin, B. Multifunctional all-in-one drug delivery systems for tumor targeting and sequential release of three different anti-tumor drugs. *Biomaterials* **2016**, *76*, 399−407.
(33) Ni, Q.; Teng, Z.; Dang, M.; Tian, Y.; Zhang, Y.; Huang, P.; Su, X.; Lu, N.; Yang, Z.; Tian, W.; Wang, S.; Liu, W.; Tang, Y.; Lu, G.; Zhang, L. Gold nanorod embedded large-pore mesoporous organo-

DOI: 10.1021/acsomega.7b01016
ACS Omega 2017, 2, 6455−6463

silica nanospheres for gene and photothermal cooperative therapy of triple negative breast cancer. *Nanoscale* **2017**, *9*, 1466−1474.
(34) Hammond, P. T. Engineering materials layer-by-layer: Challenges and opportunities in multilayer assembly. *AIChE J.* **2011**, *57*, 2928−2940.
(35) Hainfeld, J. F.; Lin, L.; Slatkin, D. N.; Dilmanian, F. A.; Vadas, T. M.; Smilowitz, H. M. Gold nanoparticle hyperthermia reduces radiotherapy dose. *Nanomed. Nanotechnol. Biol. Med.* **2014**, *10*, 1609−1617.
(36) Swierczewska, M.; Lee, S.; Chen, X. The design and application of fluorophore−gold nanoparticle activatable probes. *Phys. Chem. Chem. Phys.* **2011**, *13*, 9929−9941.
(37) Gubernator, J. Active methods of drug loading into liposomes: recent strategies for stable drug entrapment and increased in vivo activity. *Expert Opin. Drug Delivery* **2011**, *8*, 565−580.
(38) Dos Santos, N.; Mayer, L. D.; Abraham, S. A.; Gallagher, R. C.; Cox, K. A. K.; Tardi, P. G.; Bally, M. B. Improved retention of idarubicin after intravenous injection obtained for cholesterol-free liposomes. *Biochim. Biophys. Acta, Biomembr.* **2002**, *1561*, 188−201.
(39) Martinez, A. W.; Caves, J. M.; Ravi, S.; Li, W.; Chaikof, E. L. Effects of Crosslinking on the Mechanical Properties, Drug Release and Cytocompatibility of Protein Polymers. *Acta Biomater.* **2014**, *10*, 26.
(40) Bukhari, S. M. H.; Khan, S.; Rehanullah, M.; Ranjha, N. M. Synthesis and Characterization of Chemically Cross-Linked Acrylic Acid/Gelatin Hydrogels: Effect of pH and Composition on Swelling and Drug Release. *Int. J. Polym. Sci.* **2015**, *2015*, 187961.
(41) Latorre, A.; Somoza, A. Glutathione-Triggered Drug Release from Nanostructures. *Curr. Top. Med. Chem.* **2015**, *14*, 2662−2671.
(42) Collins, C. B.; McCoy, R. S.; Ackerson, B. J.; Collins, G. J.; Ackerson, C. J. Radiofrequency heating pathways for gold nanoparticles. *Nanoscale* **2014**, *6*, 8459−8472.
(43) Pantano, P.; Harrison, C. D.; Poulose, J.; Urrabazo, D.; Norman, T. Q.; Braun, E. I.; Draper, R. K.; Overzet, L. J. Factors affecting the 13.56-MHz radio-frequency-mediated heating of gold nanoparticles. *Appl. Spectrosc. Rev.* **2017**, *0*, 1−16.
(44) Li, D.; Jung, Y. S.; Kim, H. K.; Chen, J.; Geller, D. A.; Shuba, M. V.; Maksimenko, S. A.; Patch, S.; Forati, E.; Hanson, G. W. The Effect of Sample Holder Geometry on Electromagnetic Heating of Nanoparticle and NaCl Solutions at 13.56 MHz. *IEEE Trans. Biomed. Eng.* **2012**, *59*, 3468−3474.
(45) Chatterjee, K.; Zhang, J.; Honbo, N.; Karliner, J. S. Doxorubicin Cardiomyopathy. *Cardiology* **2010**, *115*, 155−162.
(46) Turkevich, J.; Stevenson, P. C.; Hillier, J. A study of the nucleation and growth processes in the synthesis of colloidal gold. *Discuss. Faraday Soc.* **1951**, *11*, 55−75.
(47) Liu, X.; Atwater, M.; Wang, J.; Huo, Q. Extinction coefficient of gold nanoparticles with different sizes and different capping ligands. *Colloids Surf., B* **2007**, *58*, 3−7.
(48) Liz-Marzán, L. M.; Giersig, M.; Mulvaney, P. Synthesis of Nanosized Gold−Silica Core−Shell Particles. *Langmuir* **1996**, *12*, 4329−4335.
(49) Singh, N.; Lyon, L. A. Au Nanoparticle Templated Synthesis of pNIPAm Nanogels. *Chem. Mater.* **2007**, *19*, 719−726.
(50) McPhee, W.; Tam, K. C.; Pelton, R. Poly(N-isopropylacrylamide) Latices Prepared with Sodium Dodecyl Sulfate. *J. Colloid Interface Sci.* **1993**, *156*, 24−30.

DOI: 10.1021/acsomega.7b01016
ACS Omega 2017, 2, 6455−6463